NINTH EUROPEAN ROTORCRAFT FORUM

Paper No. 9

PRESSURE DISTRIBUTIONS ON A HELICOPTER SWEPT TIP FROM FLIGHT TESTS AND FROM CALCULATIONS

M.J. RILEY

Royal Aircraft Establishment
(Bedford)
ENGLAND

and

JUDITH V. MILLER

Royal Aircraft Establishment
(Farnborough)
ENGLAND

September 13-15, 1983

STRESA, ITALY

Associazione Industrie Aerospaziali

Associazione Italiana di Aeronautica ed Astronautica

PRESSURE DISTRIBUTIONS ON A HELICOPTER SWEPT TIP FROM FLIGHT TESTS AND FROM CALCULATIONS

by

M.J. Riley

and

Judith V. Miller

Royal Aircraft Establishment, ENGLAND

ABSTRACT

Swept and rectangular planforms have been flight tested simultaneously on a single rotor and surface pressure distributions compared. The results demonstrate the benefit of tip sweep in suppressing supercritical flow. Comparisons with theory on the advancing blade show a large measure of agreement in the prediction of supercritical flow. Some discrepancy is evident in the initial formation of shock waves, and when present in the second quadrant, the shock waves are further back along the chord than predicted.

1 INTRODUCTION

An interest in swept tips for helicopter rotor blades began at the RAE some years ago with the development of a method for predicting the pressure distribution over blade tips in supercritical flow. Calculation indicated that substantial benefits could be obtained from sweep-back in suppressing supercritical flow over the advancing blade tip, and this led to an experimental programme to confirm these benefits. This programme was set up in collaboration with France and included model rotor tests at ONERA, which were reported at the 1982 Forum [Ref 1], and flight experiments at RAE using a Puma helicopter (Fig 1). This paper will describe these flight experiments, present some of the data obtained and compare measured and predicted pressure distributions.

2 THE DESIGN OF THE SWEPT TIP

The overall objective of the experiment was not to design the best possible tip shape, but to study the aerodynamic characteristics of a swept tip and the way in which they differ from those of a rectangular tip. Part of this study was to compare measured pressure distributions with predicted results for the advancing blade, as a check on the theory, and another part was to investigate the behaviour of a swept tip in conditions that were not amenable to theoretical treatment (eg retreating blade stall).

It was decided at the outset that a major feature of the experiment should be the measurement of surface pressures on a swept tip and a rectangular tip simultaneously. The chosen rotor configuration therefore consisted of one blade with a swept tip and the opposite blade with a dynamically balanced rectangular tip, having the same blade area and section as the swept tip. The remaining pair of blades was to be of standard design (Fig 2). With this arrangement an important design aim was to keep the centre of pressure of the

swept tip on the torsional axis of the blade to prevent any twist deformation of the blade that was not experienced by the opposite blade with its rectangular tip. This was to ensure that the operating conditions of the two tips were as near identical as possible. Furthermore, as the new tip was to be built on to an existing blade it was important that the aerodynamic and dynamic loads differed as little as possible from those for a standard blade.

To meet the above constraints, the swept tip was designed to have a leading-edge extension inboard of the swept back portion, as shown in Fig 3. As this tip had an increased chord and area, relative to a standard blade tip, the opposite rectangular tip had to have the same increases in these quantities. With an increased chord on both tips, it was necessary to design a new aerofoil section with reduced thickness/chord ratio so as to avoid an excessive increase in tip volume and mass. A symmetric section was designed that could envelop the basic blade spar over as large an extent of span as possible (see Fig 4) and this section was defined in the plane normal to the blade axis for both tips. Thus differences between the two tip shapes were in planform only.

To confirm that a significant aerodynamic improvement should be achieved with the swept tip, calculations of the pressure distributions were made on both swept and rectangular tips. For this purpose the method described in Ref 2 was used. This solves the transonic small perturbation approximation to the inviscid potential equation for the flow around the tip region of the blade. The program calculates three-dimensional quasi-steady cases, which are used to give a reasonable prediction of the flow for a useful range of azimuth angles around $\psi = 90^{o}$. It is also possible to run lifting cases, for which the wake is modelled by a plane vortex sheet skewed in the direction of the freestream velocity, but a spanwise distribution of incidence is required for the calculation. In practice the incidence at the tip of the advancing blade is normally small, and the swept tip was designed on the basis of calculations at zero lift.

Theoretical calculations were performed for a blade with the swept tip planform and also for a rectangular blade assuming the increased blade chord of the rectangular tip, and its section, to be constant along the blade. The detailed geometry of the inboard end of the rectangular tip planform was not modelled, but this was not thought to have any significant effect on the results in the tip region. For both the swept tip blade and the rectangular blade, the inboard boundary for the calculation was taken to be 3.8 chord-lengths from the tip, which corresponds to a station at about 70% rotor radius. At this boundary it is assumed that there is no perturbation to the flow in the direction normal to the local freestream direction. The contours of p/H_0 from the computation at $\psi = 90^{o}$ are shown in Fig 5 for a case with a blade tip Mach number of 0.675 and a forward speed of 160 knots. The shock wave that is predicted to occur towards the tip of the rectangular blade at about 40% chord has vanished on the swept tip, where minimum pressures are appreciably higher.

The design of the blade structural modifications, necessary for the incorporation of the swept tip, was carried out by Aerospatiale who also built a set of four modified blades. A final balsa wood and glass-fibre skin was added to the tip at the RAE with pressure sensors and wiring embedded in the skin of one of the blades. This instrumented swept tip blade was the only one to be used in the first phase of the experiment. The next phase will concentrate on tests with swept tips on all four blades.

3 MEASUREMENT TECHNIQUES

In this first phase of the experiment 68 pressure sensors were installed along four chordlines on the swept tip and a further 44 sensors along three chordlines on the rectangular tip, as shown in Fig 3. In addition, loads were measured for airworthiness purposes by strain gauges at 17 points on the blades and control system. The blade root motions and control inputs were also recorded so that the trim of the helicopter could be fully defined. The airborne recording equipment used a pulse code modulated (PCM) digital system which recorded the data from two complete rotor revolutions. The signals were amplified at the rotor head before being multiplexed and passed through slip rings. However, the high sampling rate combined with the large number of channels required the use of a solid state buffer memory to store the data before it was written to a digital magnetic tape recorder. Signal processing on the ground was through the DATAMAP graphics and analysis system [Ref 3]. The unusual rotor configuration required continuous monitoring of certain rotor parameters to ensure safety in flight. The data was telemetered to ground observers who were in contact with the pilot so that potentially dangerous conditions could be avoided.

The operation of the Puma helicopter with the experimental blades has so far proved to be less of a problem than was at first anticipated, considering the different blade weights and planforms incorporated. The design principle, to avoid dynamic and aerodynamic coupling where possible, enabled the aircraft to be flown with acceptable vibration levels throughout the normal flight envelope. Control loads were generally higher on both experimental blades than on the standard blades, but they were considered acceptable using the continuous load monitoring to account for the extra fatigue damage sustained. An increase in the maximum speed and variations in the rotor speed provided small extensions to the normal flight envelope, which were used to study the trends with Mach number more thoroughly.

4 FEATURES OF THE BLADE TIP LOADING

The effect of the sweep of the blade tip can be assessed most clearly from a comparison of the measured and predicted chordwise pressure distributions on the two tips, but it is important to view the overall blade loadings in the tip region for each flight condition analysed. Fig 6 shows the way in which the blade lift varies around the azimuth for each radial position. Note that for this flight condition (155 knots forward speed) at around $\psi = 90^{\circ}$ on the advancing blade, the lift is small and the swept tip loading closely matches that on the rectangular blade tip at each azimuth angle. Similarly in Fig 7 the pitching moments measured about the local quarter chord point are also compared. In the advancing blade region the pitching moments of the two tip shapes are reasonably similar. It must be emphasised however, that the automatic derivation of pitching moments from pressure distributions with strong shocks can lead to errors, even though a relatively large number of sensors were used on each chordline. The majority of the sensors were placed in the first half of the chordline where the shocks were expected to occur in flight. However, flight conditions were encountered where the shocks moved further back than anticipated before causing shock-induced separation, and thus were in a region having few sensors.

More detail of the pressure distributions can be shown by the time histories of individual pressure sensors. In Fig 8 the two blade tips are compared by selecting sensors which reveal the strength and location of the

shocks on each tip at 0.95 radius. Careful analysis of these plots, each of which has 256 samples for one revolution of the rotor, can define the extent of the supercritical flow more precisely than is possible from each chordwise distribution directly. In effect, the measurement technique uses a rapid sampling rate in a dynamic situation to overcome the problem of having a limited number of sensors. Fig 8 shows only one chordline from each blade, but similar plots at each of the seven chordlines provide a complete picture of the supercritical flow areas over the tip region of both blades. In Fig 8 the suppression of the supercritical flow on the swept tip is immediately apparent. The swept tip has reduced both the shock strengths and the extent of supercritical flow around the azimuth. When supercritical flow is present, the shock wave moves backwards and forwards along the blade chord as the azimuth angle changes. The sudden change in pressure recorded by a sensor is a result of the shock wave passing over that sensor. Thus, by noting the azimuth angle at which this sudden change occurs, it is possible to plot the variation of shock position with azimuth. The shock position for any particular chordwise pressure distribution can then be read off and used in fitting a curve to the measured pressures. A similar analysis can be performed for the shock strength.

A further illustration of the versatility of the DATAMAP graphics system is demonstrated in Fig 9 by the contours of p/H_0 on each tip. The sharp pressure gradients associated with the strong shock on the rectangular tip are replaced by a much more gradual variation of pressure, with no shocks apparent on this example which was measured at 60° azimuth.

5 BLADE DYNAMIC RESPONSE

In this experiment care was taken in the design of the swept tip to avoid, as far as possible, any significant differences between dynamic responses of the blades with swept and rectangular tips. However, it was found that both these blades were subjected to a higher harmonic variation of blade twist that was sufficient to produce a significant variation of incidence at the tip. The twist variation is implied by the measured variation of pitch link load shown, for the swept tip, at the top of Fig 10. The four peaks in pitch link load at 40°, 160°, 270° and 335° azimuth correspond to local increases in incidence at the tip. The output of the pressure sensors at 4% chord and 10% chord show that this incidence perturbation leads to the appearance of separate supercritical flow regions in each of the first and second quadrants of the rotor disc. The region around 90° has very little supercritical flow. To establish simple test cases for the initial comparison with flow calculations, flight conditions were sought where the blade twisting was small in order to minimise the superimposed variation of incidence outlined above. High speed autorotation was found to give the required high Mach number with considerably reduced twisting and these examples are used in the comparisons with prediction in this paper. However, the results for powered high speed flight show that the greatest penetration into supercritical conditions does not necessarily occur close to 90° azimuth, and this must be borne in mind when designing a swept tip.

Before turning to detailed comparisons of the performance of the tips in the advancing blade region, pressure distributions measured in flight at four points around the rotor disc are included in Fig 11. The critical conditions have been indicated at $p/H_0 = 0.528$ for the rectangular tip, but for

the swept tip conditions normal to the leading-edge have been considered, as discussed by Wilby [Ref 4]. This approach results in a critical value of p/H_0 which depends on the flight conditions, and varies with azimuth as shown in the diagram. For this level flight condition the reduction in supercritical flow on the swept tip is evident at 90° azimuth. At 180° azimuth the pressures on the swept tip are rather lower than on the straight tip, as would be expected if the freestream Mach number were higher, following the trend noted in the model rotor tests [Ref 1]. Pressure distributions are little different at 270° azimuth although it is interesting to note that the leading-edge suction peak is lower for the swept tip. Conditions are supercritical at 360° azimuth, the straight tip having a shock wave that is stronger and further aft than on the swept tip. This is explained by the fact that, at this azimuth, sweepback leads to a reduction in the component of incident flow Mach number normal to the leading-edge (the reverse is true at $\psi = 180°$) as pointed out in Ref 1. These differences in pressure distribution, especially at the rear of the rotor disc, emphasise the importance of studying the performance of the swept tip blade at all other azimuth angles as well as in the obvious advancing blade region.

6 COMPARISON OF MEASURED AND PREDICTED RESULTS

One of the objectives of the experiment was to check on whether or not the predicted advantages of the swept tip for the advancing blade were realized in practice. An important part of the data analysis is therefore a comparison of measured and predicted pressure distributions. It is however difficult to obtain a direct comparison between experiment and theory because the rotor blade operates under lifting conditions and it is not possible to measure blade aerodynamic incidence in the flight tests. However, incidence near the tip of the advancing blade is normally close to zero. A useful comparison can thus be made by plotting measured pressure distributions for swept and straight tips alongside predicted distributions, at zero lift, for both tips as in Figs 12 to 15. For these cases the lift coefficient over the outer part of the experimental tip is approximately 0.1. Critical conditions have been indicated at $p/H_0 = 0.528$, which is valid for the rectangular tip only.

The comparison in Fig 12 is for a flight case with tip Mach number equal to 0.68 and a (true) forward speed of 140 knots, at an altitude of 8000 ft. The diagram shows the measured pressure distributions from the flight experiment on the left and the corresponding theoretically predicted distributions on the right, for three radial stations at 90° azimuth. For the most inboard station, at the bottom of the diagram, only the upper surface pressures are available from experiment, and the amount of lift present is not known. This should be borne in mind when looking across the diagram. In general, both sets of results indicate the advantages to be gained from the swept tip, in the reduction of supercritical flow over the blade, and in the decreased shock strength at the end of the supercritical region. However, the measured effect of sweepback is not quite as large as is predicted. This seems to be due to differences between predicted and measured pressures on the swept tip (with a shock wave appearing in practice in place of the predicted isentropic recompression) rather than differences in the two sets of results for the rectangular tip. This is borne out in Fig 13, which compares the predicted non-lifting results with a pressure distribution which is obtained as the mean of upper and lower surface values from experiment, in a flight case in which the tip Mach number was 0.67 with a speed of 155 knots. The comparison is made at 95% rotor radius, at 90° azimuth, where very little lift was generated. While the minimum

pressure is approximately the same for the swept tip in each case, the experimental results again show a shock wave that was not given by theory. For the straight tip, the exact position and strength of the shock is difficult to judge, because of the lack of sensors over the rear of the blade, but the correspondence between theory and experiment is still much better than for the swept tip.

In Fig 14, pressure distributions are shown at 95% rotor radius for a range of azimuth angles on the advancing side of the disc. The flight conditions this time were as in Fig 12. The beneficial effects of the swept tip are again demonstrated both in theory and in flight at each value of azimuth. For the swept tip, no shock is predicted or measured at $\psi = 60^{o}$, but a shock is present in flight at $\psi = 90^{o}$ and at $\psi = 120^{o}$ whereas theory gives an isentropic recompression. The comparison between theory and experiment at $\psi = 120^{o}$ is particularly interesting as the experimental conditions are very close to zero lift for both swept and straight tips. Here the shock wave is much further back along the chord in experiment than in theory. This is recognised as being one of the effects of unsteady Mach number terms that are omitted in the present calculations [Ref 2]. At RAE, the effort in computing unsteady flow has been concentrated on two-dimensional problems, but a three-dimensional unsteady program has been written at ONERA [Ref 5].

The next comparisons of experiment with theory in Fig 15 show the pressure distributions at 0.95R, $\psi = 90^{o}$, for three different Mach numbers. The central case is the same as in Figs 12 and 14. The lowest Mach number case, at the bottom of the diagram, has a tip Mach number of 0.62 and a flight speed of 155 knots. For this case, the predicted shock on the straight tip is smeared and further forward than in experiment. The swept tip comparison is better than in the previous diagrams, but there is only a small supercritical region apparent in experiment and in theory. The higher Mach number case at the top of the diagram is again at 155 knots, with an increased tip Mach number of 0.69. Now the predicted shock on the swept tip is smeared and further forward than in experiment. The evidence would seem to suggest that the theory is not good at predicting the early formation of shocks on either planform, and it is not just the treatment of the swept tip which is questionable. However, the overall trend of the supercritical region extending further back over the blade with increased Mach number, is portrayed in both theory and experiment for both shapes of tip.

Finally, some calculations were made with non-zero incidence to obtain lift coefficients similar to those in experiment, for the same flight case as in Fig 12. The pressure distributions are shown in Fig 16, and comparison with the experimental results on the left-hand-side of Fig 12 highlights the tendency, present in the previous diagrams, of the calculated minimum pressure on the swept tip to be further forward than in the flight measurements, and of the shock to be smeared or treated as an isentropic recompression. This phenomenon is not as prevalent in the rectangular tip calculations, but supercritical flow is further developed on this tip than on the swept tip, and it has already been suggested that inaccuracies in the theory may be most apparent in the initial stages of shock formation.

7 CONCLUSIONS

The concept of flying a rotor having blades of different tip shapes has proved to be practical and successful throughout the whole flight envelope, with fewer balance problems than anticipated.

Considerable benefits of a swept tip in suppressing supercritical flow on the advancing blade have been demonstrated in true flight conditions.

In general, the calculations predicted the supercritical flow well, but the measured benefits were not quite as large as predicted. This appears to be due to inadequacies in the ability of the theory to predict the initial formation of a shock wave.

In high speed powered flight, twist deformations have been shown to be particularly important in controlling the variation of supercritical flow with azimuth.

In the second quadrant of the disc the shock wave (when present) is found to lie further back on the chord than is predicted, supporting earlier evidence on the importance of unsteady terms in the theory.

Tests with all four blades having swept tips will continue shortly and will include overall rotor performance measurements.

REFERENCES

1 P.G. Wilby and J.J. Phillipe: An investigation of the aerodynamics of an RAE swept tip using a model rotor.
Proceedings of the 8th European Rotorcraft Forum, Aix-en-Provence, September 1982.

2 J. Grant: The prediction of supercritical pressure distributions on blade tips of arbitrary shape over a range of advancing blade azimuth angles.
Proceedings of the 4th European Rotorcraft and Powered Lift Aircraft Forum, Stresa, September 1978. Vertica, Vol 3, pp 275-292, 1979.

3 R.B. Philbrick: The data from aeromechanics test and analytics management and analysis package (DATAMAP) Vol I - User's manual, Vol II - Systems manual.
USAAVRADCOM TR 80-D-30A and 30B (1980)

4 P.G. Wilby and J.J. Phillipe: An investigation of the aerodynamics of an RAE swept tip using a model rotor.
Proceedings of the 39th Annual AHS Forum, St. Louis, Missouri, May 1983.

5 J.J. Chattot: Calculation of three-dimensional unsteady transonic flow past helicopter blades.
NASA TP 1721, AVRADCOM TR 80-A-2 (AM), 1980.

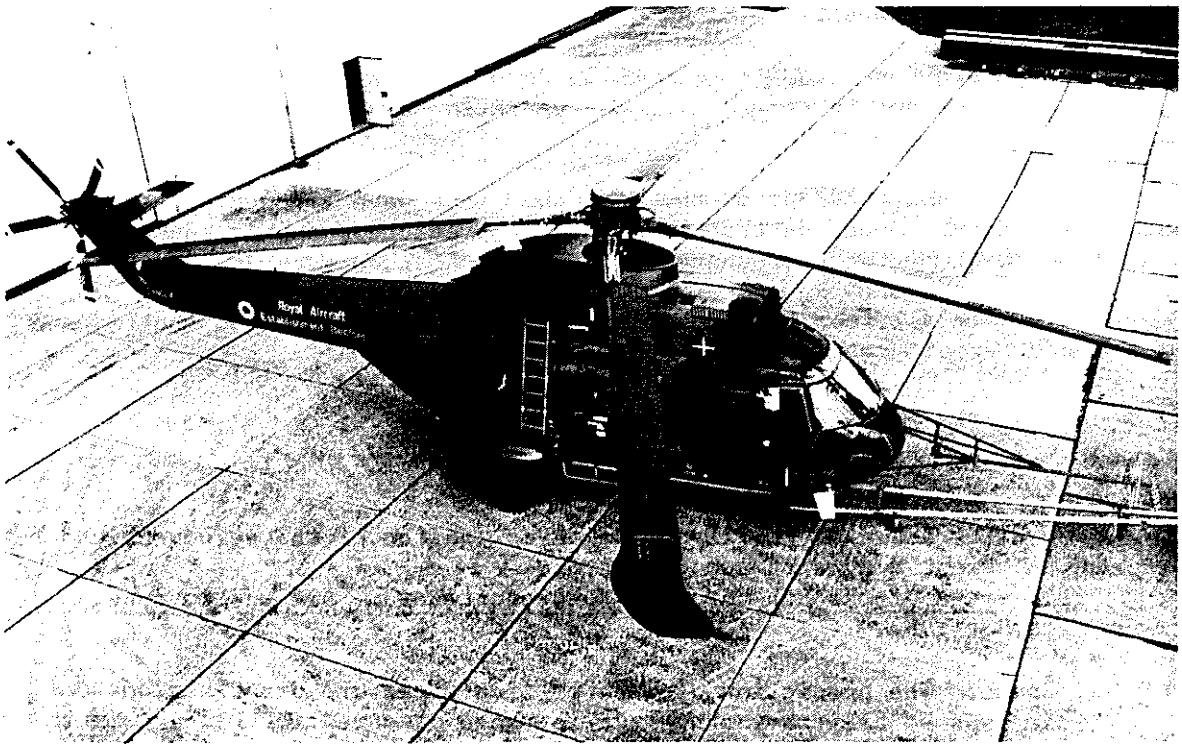

Fig 1 RAE Puma with swept-back blade tip

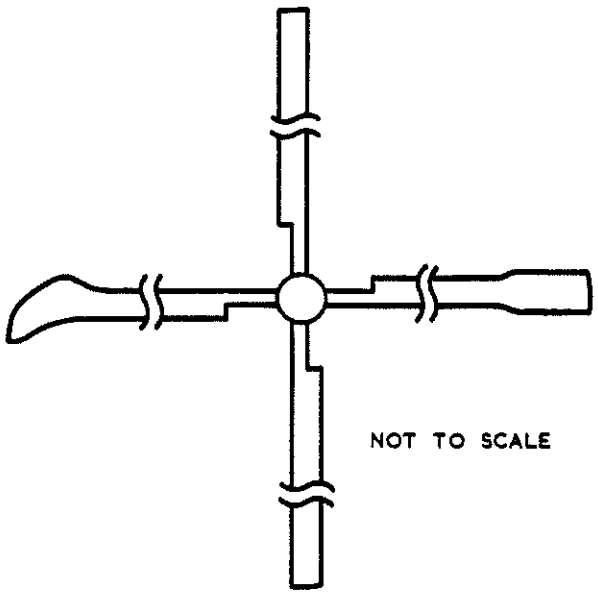

Fig 2 Rotor configuration with swept and rectangular tips

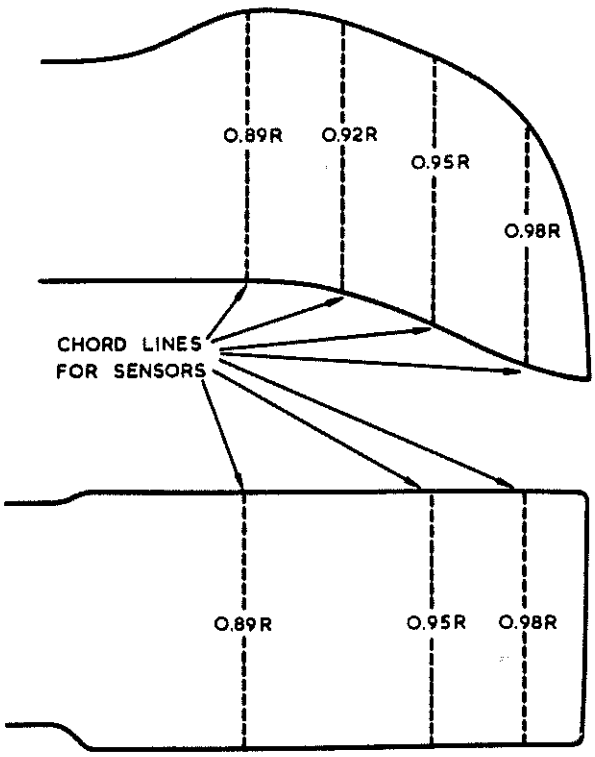

Fig 3 Planform for swept and rectangular tips

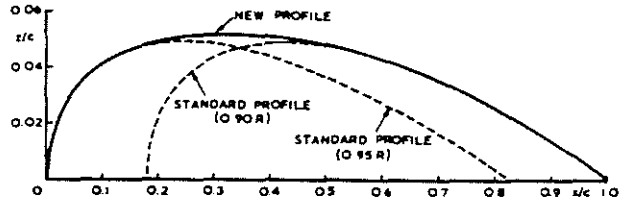

Fig 4 Profile for swept tip in relation to Puma blade section

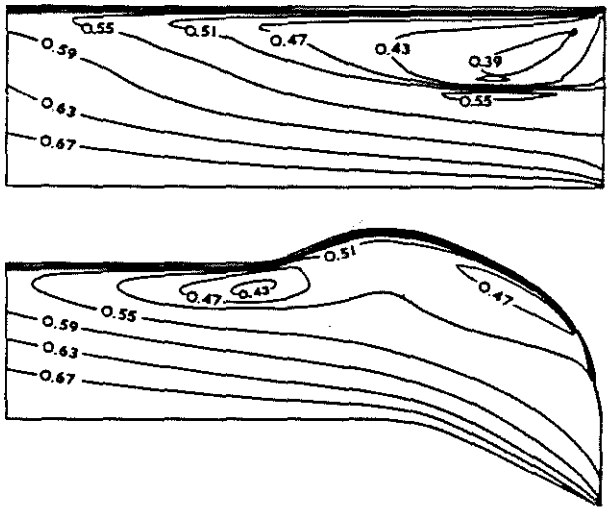

Fig 5 Predicted isobars for straight and swept tips

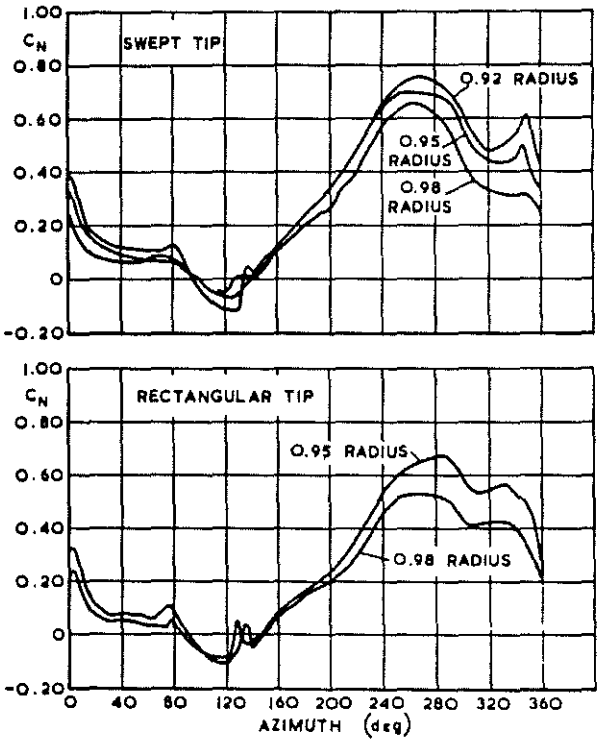

Fig 6 Normal force coefficients measured at each radius

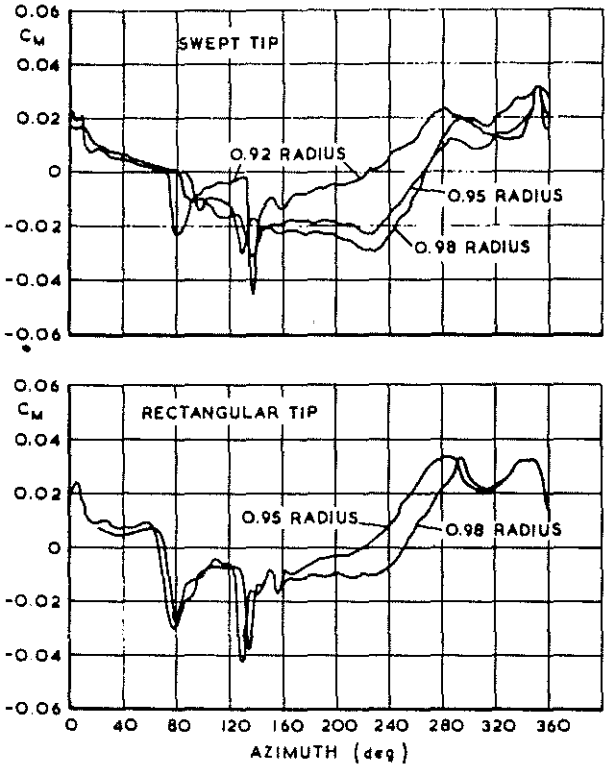

Fig 7 Pitching moment coefficients measured at each radius

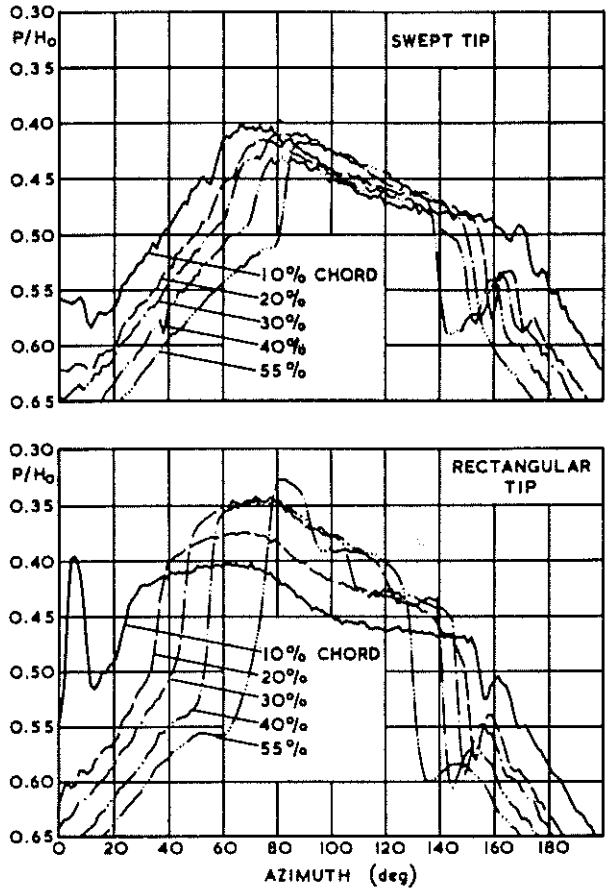

Fig 8 Pressure measurements showing shock positions on upper surface at 0.95 radius

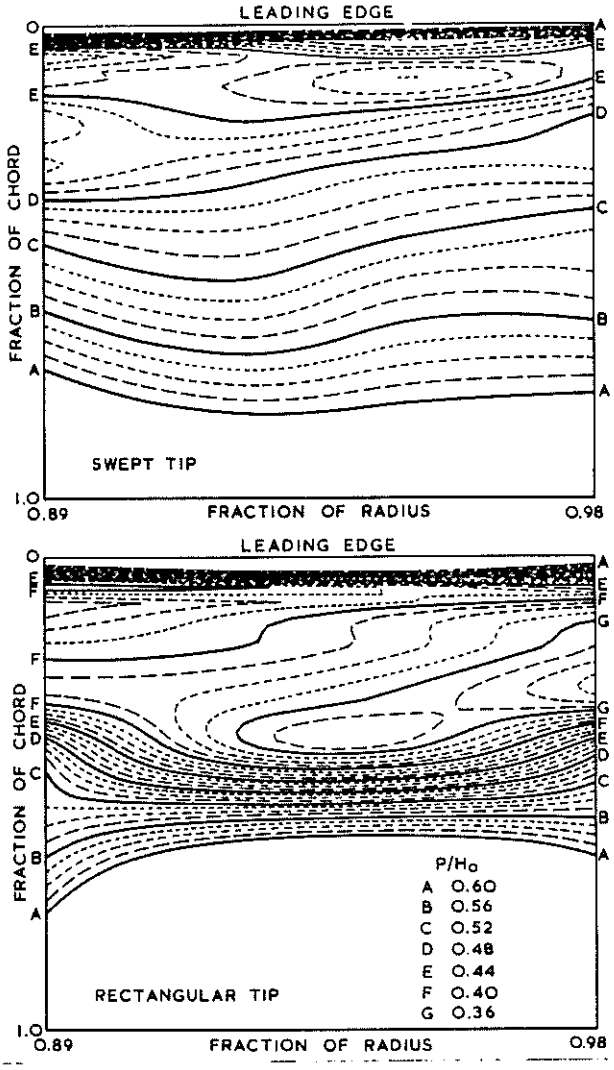

Fig 9 Measured isobars for swept and rectangular tips at 60 degrees azimuth

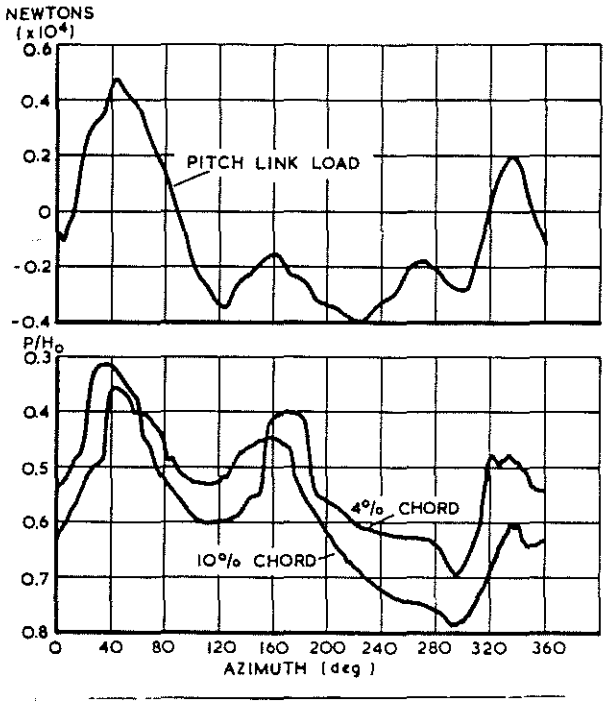

Fig 10 Correlation of blade twisting with supercritical flow on swept tip

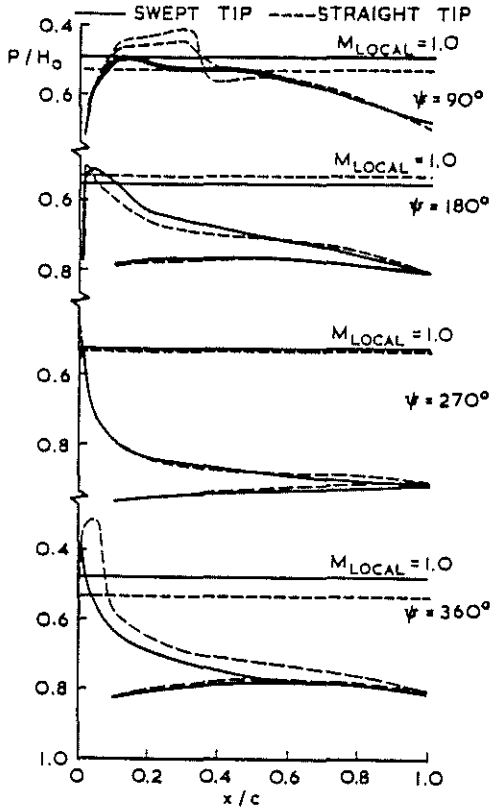

Fig 11 Pressure distributions measured on swept and straight tips (M_T = 0.615, μ = 0.385)

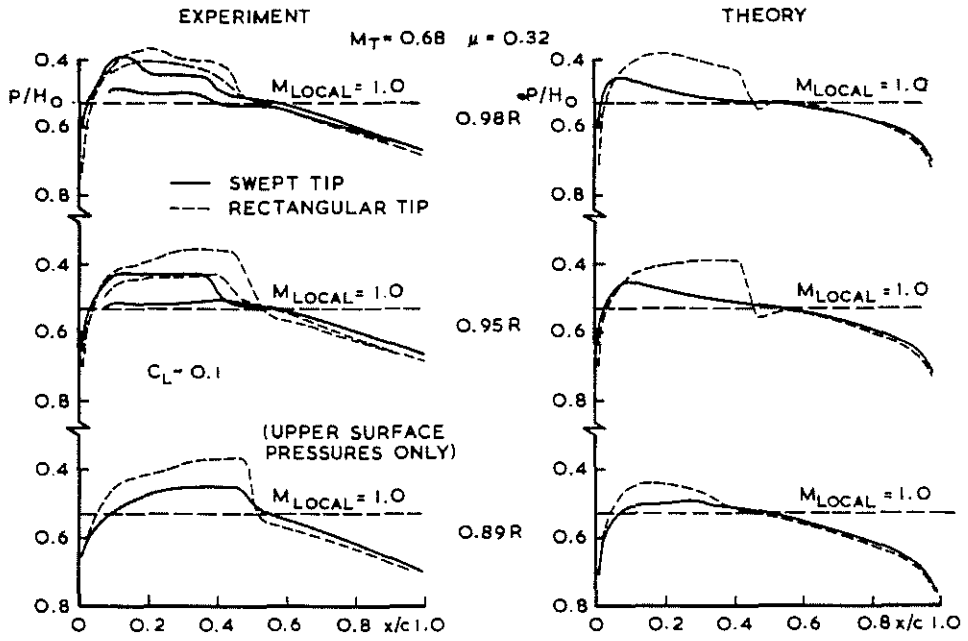

Fig 12 Measured and predicted pressure distributions at $\psi = 90^0$ for range of spanwise positions

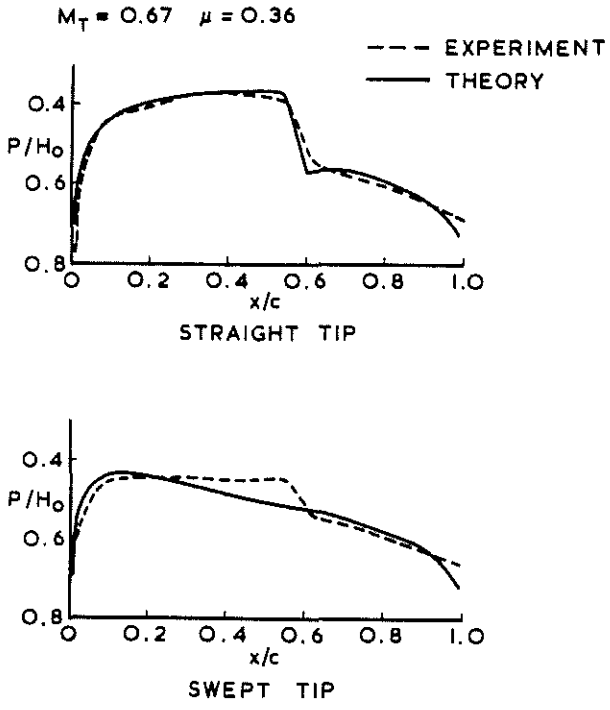

Fig 13 Predicted and mean measured pressure distributions at $\psi = 90^0$, 0.95R for straight and swept tips

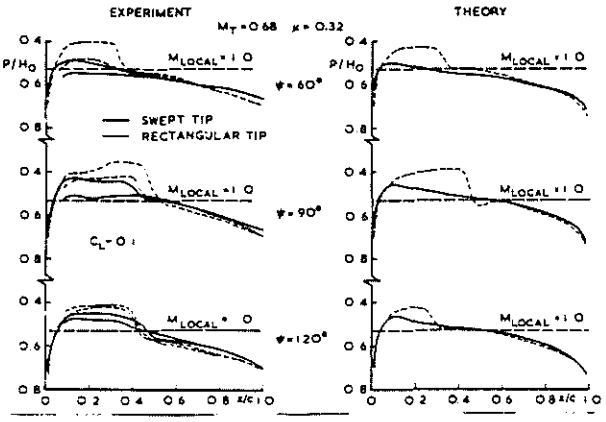

Fig 14 Measured and predicted pressure distributions at 0.95R for range of azimuth angles

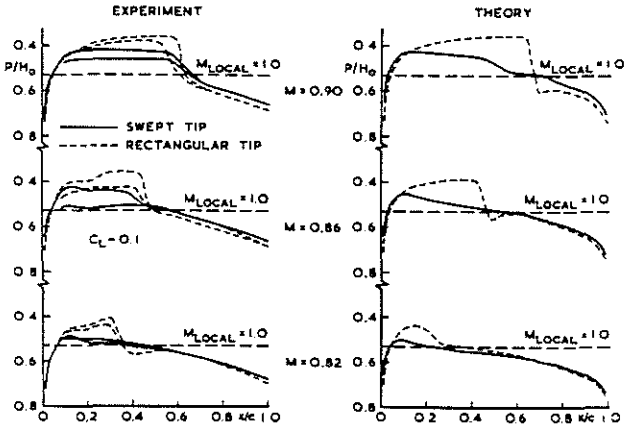

Fig 15 Measured and predicted pressure distributions at 0.95R for range of Mach number at $\psi = 90^0$

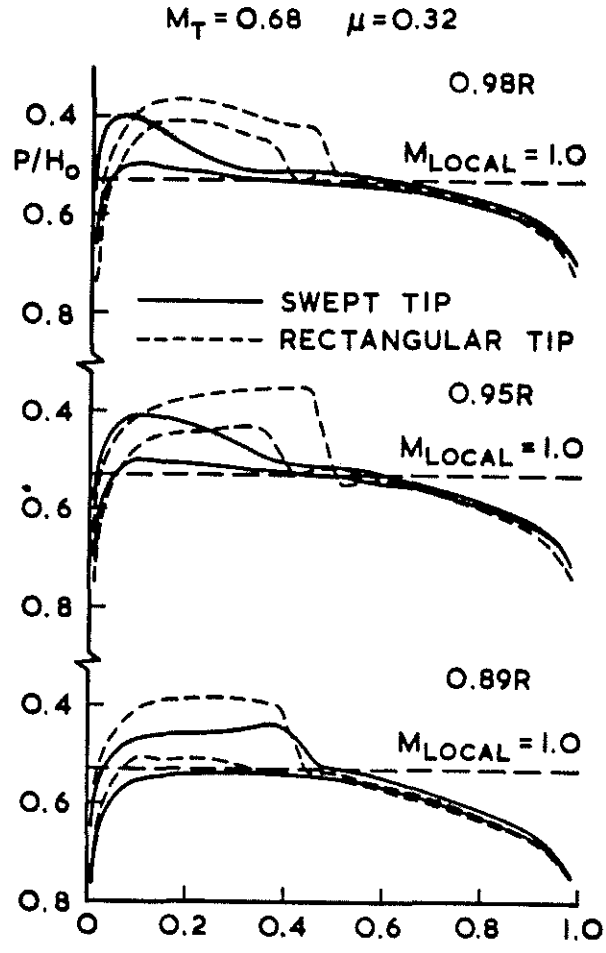

Fig 16 Predicted pressure distributions for lifting blades at $\psi = 90^0$ for range of spanwise stations